第37卷第2期 2021年2月
无 机 化 学 学 报 CHINESE JOURNAL OF INORGANIC CHEMISTRY
Vol.37 No.2 327-339

# $MoSe_2/Ag_3PO_4$复合材料的制备及其可见光降解罗丹明B的光催化性能

王新刚[1,2] 刘 凯[1,2] 朱 晖[1,2] 李翀煜[1,2] 林雷雷[1,2] 郭 峰*[,1,2] 代洪亮*[,1,2,3]
([1]江苏科技大学环境与化学工程学院,镇江 212003)
([2]江苏科技大学海洋装备与技术研究院,镇江 212003)
([3]华中科技大学环境科学与工程学院,武汉 430074)

**摘要:** 通过原位沉积法合成了一种光催化活性强、稳定性高的$MoSe_2/Ag_3PO_4$复合材料。$MoSe_2/Ag_3PO_4$形成的异质结构能有效分离光生电子-空穴对,从而提高光催化活性。光生电子从$Ag_3PO_4$表面向$MoSe_2$的转移降低了$Ag^+$向金属Ag的可能性。当$MoSe_2$和$Ag_3PO_4$的质量分数为1∶5(最优组合)时,$MoSe_2/Ag_3PO_4$在可见光照射下30 min内降解RhB效率达98%,并且经过4次重复试验,其可见光照射下RhB降解效率仍可达到89%。通过液相色谱/质谱(LC/MS)技术测定光催化过程中产物的变化,提出了$MoSe_2/Ag_3PO_4$光催化降解RhB的途径。

**关键词:** 光催化; 染料; 硒化钼; 磷酸银; 光降解
**中图分类号:** TQ139.2 **文献标识码:** A **文章编号:** 1001-4861(2021)02-0327-13
**DOI:** 10.11862/CJIC.2021.038

# $MoSe_2/Ag_3PO_4$ Composites: Preparation and Photocatalytic Properties for Degradation of Rhodamine B under Visible Light

WANG Xin-Gang[1,2] LIU Kai[1,2] ZHU Hui[1,2] LI Chong-Yu[1,2]
LIN Lei-Lei[1,2] GUO Feng*[,1,2] DAI Hong-Liang*[,1,2,3]
([1]*School of Environmental and Chemical Engineering, Jiangsu University of Science and Technology, Zhenjiang, Jiangsu* 212003, *China*)
([2]*Marine Equipment and Technology Institute, Jiangsu University of Science and Technology, Zhenjiang, Jiangsu* 212003, *China*)
([3]*School of Environmental Science and Engineering, Huazhong University of Science and Technology, Wuhan* 430074, *China*)

**Abstract:** The as-prepared $MoSe_2/Ag_3PO_4$ by *in-situ* deposition showed favorable photocatalytic activity and stability. Heterostructure of $MoSe_2/Ag_3PO_4$ had efficient separation of photogenerated electron-hole pairs that led to the elevated photocatalytic activity. The transfer of photogenerated electrons from the surface of $Ag_3PO_4$ to $MoSe_2$ reduced the possibility of $Ag^+$ to metallic Ag. When the mass ratio of $MoSe_2$ and $Ag_3PO_4$ was 1∶5 (champion combination), the obtained $MoSe_2/Ag_3PO_4$ could reach to 98% for RhB degradation under visible light irradiation within 30 min. In addition, $MoSe_2/Ag_3PO_4$ still achieved 89% of the degradation under visible light irradiation after four regenerations. Eventually, the photocatalytic degradation of RhB by $MoSe_2/Ag_3PO_4$ was revealed by liquid chromatography/mass spectrometry (LC/MS).

**Keywords:** photocatalysis; dyes; $MoSe_2$; $Ag_3PO_4$; photodegradation

收稿日期:2020-05-19。收修改稿日期:2020-12-08。
国家自然科学基金项目(No. 51908252)、中国博士后基金面上项目(No. 2019M652274)、江西省博士后基金择优资助项目(No.2019KY17)、江苏省研究生科研与实践创新项目(No.SJCX19_1198)、镇江社会发展项目(No.2016014)、江苏省高校青年骨干教师青蓝工程项目和江苏科技大学海洋装备与技术研究院项目(No.HZ20190004)资助。
*通信联系人。E-mail:gfeng0105@126.com,daihongliang@just.edu.cn

## 0 Introduction

With rapid industrialization and growing population, environment pollution has become the greatest challenge for human being in modern society. Sunlight-driven semiconductor photocatalysis is a "green" and promising environmental remediation technology. Semiconductor photocatalysis technology uses sunlight as an energy source and semiconductor materials as a photocatalyst[1-3]. Converting light energy into other energy, oxygen and water molecules stimulate city free radicals[4-5]. The free radical has high oxidizing property and can effectively degrade organic pollutants adsorbed on the surface of the catalyst[6-7]. It is a novel and environmentally friendly treatment technology, and has potential application prospects in the degradation of dye wastewater in recent years[8-9].

In 2010, Ye′s research group reported that silver phosphate ($Ag_3PO_4$) can absorb sunlight with a wavelength of less than 520 nm and has a quantum yield more than 90%[10]. Although $Ag_3PO_4$ shows strong advantages in terms of catalysis, it still has a series of drawbacks including higher cost of $Ag_3PO_4$ preparation and poor photocatalytic stability. The photocatalytic effect of $Ag_3PO_4$ decreases significantly restricting its development in the field of photocatalysis with the increase of cycle times[11-13]. Photoelectrons are generated due to the microscopic $Ag_3PO_4$ in water when the catalyst is exposed to light. The dissolved $Ag^+$ will be reduced to Ag, and Ag deposits on the surface of the catalyst, which hinders the light absorption of the catalyst. Therefore, the modification of $Ag_3PO_4$ has become a research hotspot[14].

The transition metal chalcogenide is a generic term for compounds composed of transition metal atoms and chalcogenide atoms. Many of them have a structure similar to graphite[15]. Studies have shown that transition metal chalcogenide nanomaterials have a narrow band gap. Therefore, they have a wide range of applications in catalysis, battery electrodes, lubrication, sensors and water treatment[16-17]. At present, a variety of ligands and $Ag_3PO_4$ compound materials have been prepared because they have excellent effects in the field of photocatalytic degradation. Such as $Ag_3PO_4$/$MoO_3$[18], $BiVO_4$/RGO/$Ag_3PO_4$[19], $Ag_3PO_4$/GO[20], g-$C_3N_4$/Carbon nanotubes/$Ag_3PO_4$ (g-$C_3N_4$/CNTs/$Ag_3PO_4$)[21]. Layer-structured transition metal dichalcogenides like $MoS_2$ and $MoSe_2$ have been tested as photocatalysts, due to their unique structures, narrow band gaps and weak Van der Waals interactions between neighboring layers[22-23]. Molybdenum selenide ($MoSe_2$) is composed of Mo atoms sandwiched between two layers of hexagonally close-packed Se atoms in a layered structure with a band gap of 1.7~1.9 eV. Furthermore, $MoSe_2$ possesses a high resistance to photo-corrosion, as the optical transitions are between nonbonding metal states. $MoSe_2$ is a semiconductor material with good electron mobility, which can combine with $Ag_3PO_4$ to transfer electrons using the high electron mobility of $MoSe_2$ to reduce the formation of Ag element, thus improving the recycling capacity of the catalyst[24].

In this work, we aimed to synthesize a novel $MoSe_2$/$Ag_3PO_4$ photocatalyst through a facile and mild hydrothermal approach. The photocatalytic activity was evaluated by the degradation of RhB under the visible light ($\lambda$>420 nm) irradiation. Scan electron microscope (SEM), X-ray diffraction (XPS), X-ray photoelectron spectroscopy (XRD) and UV-Vis was used to detect the characteristics of the as-prepared materials. The photocatalytic mechanism of the $MoSe_2$/$Ag_3PO_4$ was investigated by the radical trapping experiments. The photogeneration intermediates products were analyzed using liquid chromatography/mass spectrometry (LC/MS) technology. The photocatalytic cycling experiments were employed to assess the stability of photocatalysts.

## 1 Experimental

### 1.1 Materials

All chemicals in this study were of analytical grade without any further purification. Selenium powder (Se), sodium molybdate ($Na_2MoO_4\cdot 2H_2O$), silver nitrate ($AgNO_3$), sodium hydroxide (NaOH), hydrochloric acid (HCl, mass fraction of 36%), absolute ethanol ($C_2H_6O$), dibasic sodium phosphate ($Na_2HPO_4$) were obtained from Sino Pharm Chemical Reagent. Sodium borohydride ($NaBH_4$) was obtained from Rich Joint Co., Ltd.

### 1.2 Synthesis of $MoSe_2$

Synthesis of $MoSe_2$ by hydrothermal method. In a typical synthesis, 0.225 g $NaBH_4$, 0.476 5 g $Na_2MoO_4$ and 0.311 g Se powder dissolved into 80 mL deionized water stirring for 60 min to produce a uniform dispersion. The resulting solution was poured into a 100 mL Teflon-lined stainless-lsteel reactor and treated at 220 ℃ for 24 h. The upper liquid was poured out, and the bottom black product was collected, centrifuged and washed multiple times, in order to remove the excess selenium in the reaction, and the dried black powder was added to 60 mL NaOH solution and treated at 80 ℃ for 2 h. After cooling naturally to room temperature, the supernatant liquid was poured off, and the bottom product was collected, washed 6 times with deionized water and anhydrous alcohol, and finally dried at 80 ℃ for 24 h to obtain $MoSe_2$[25-28].

### 1.3 Synthesis of $MoSe_2/Ag_3PO_4$

A typical $MoSe_2/Ag_3PO_4$ heterojunction was prepared as follows: 20 mg as-prepared $MoSe_2$ was dispersed in 30 mL deionized water and the solution was sonicated for 30 min to obtain a uniform black dispersion. The $AgNO_3$ solution was magnetically stirred and added dropwise to the dispersion. After the addition was completed, the solution was stirred for 60 min, so that $Ag^+$ can be fully absorbed on the surface of $MoSe_2$, and then the $Na_2HPO_4$ solution was added drop by drop. Magnetic stirring continued for 2 h after the addition was completed, then the supernatant was decanted, and the bottom product was collected. The product was washed three times with alcohol and dried in the dark at 60 ℃ for 12 h to obtain the $MoSe_2/Ag_3PO_4$ complex, prepared according to the amount of control $AgNO_3$ and $Na_2HPO_4$ solution. The mass ratios of $MoSe_2$ and $Ag_3PO_4$ were 1∶20, 1∶10, 1∶5, 1∶1 and 2∶1. The color of the complex gradually deepened with increasing $MoSe_2$ content. As a comparison, pure $Ag_3PO_4$ was prepared without addition of $MoSe_2$.

### 1.4 Characterization

$MoSe_2/Ag_3PO_4$ composite (1∶5) was used in the characterization. The photocatalysts were analyzed by XRD on a Bruker D8 diffractometer employing Cu $K\alpha$ radiation ($\lambda$=0.154 07 nm, 40 kV, 40 mA, 5 (°)·$min^{-1}$ from 10° to 80°). Elemental compositions were determined by XPS on an ESCALAB 250 Xi X-ray photoelectron spectrometer employing Mg $K\alpha$ radiation. The morphology and structure of as-prepared samples were analyzed using a SU 8220 field emission SEM and an S-4800 (Hitachi, Japan) operating at 30 kV. UV-Vis absorption spectra of the samples were measured on a UV-Vis spectrophotometer (Shimadzu UV-2450, Japan) in a range of 200~800 nm with fine $BaSO_4$ powder as reference.

### 1.5 Photocatalytic experiment

$MoSe_2/Ag_3PO_4$ hybrid materials samples have been evaluated under the visible light irradiation for RhB degradation. Before the irradiation, the solutions have been stirred to achieve absorption - desorption equilibrium in the dark. At the setting intervals, 5 mL suspension has been taken out and analyzed with an UV-Vis spectrophotometer (Shimadzu UV-2450) at 554 nm.

The photocatalytic degradation efficiency ($E$) was obtained by the following formula:

$$E=\left(1-\frac{c}{c_1}\right)\times 100\%=\left(1-\frac{A}{A_1}\right)\times 100\% \quad (1)$$

The kinetic constant ($k$) was obtained by the following formula:

$$-\ln\left(\frac{c}{c_0}\right)=kt \quad (2)$$

Where $c$ is the concentration of RhB at different times, $c_1$ is the initial concentration of RhB, $c_0$ is the initial concentration of RhB after adsorption equilibrium, $A$ and $A_1$ are the corresponding absorbances.

### 1.6 Active species capturing experiment

Scavengers were added in the photocatalytic degradation process of RhB, where 2-propanol, ammonium oxalate and benzoquinone were added into the photocatalytic test to capture hydroxyl radicals (·OH), holes ($h^+$) and superoxide radicals ($\cdot O_2^-$), respectively.

### 1.7 Analysis of the photogeneration intermediates

LC/MS technology was used to identify intermediates in the photocatalytic oxidation of RhB. The photogeneration intermediates in the RhB solution were separated by high-performance liquid chromatography (Ultimate 3000 UHPLC-Q Exactive, Thermo Scientific,

USA), using a C18 reversed phase column (100 mm× 4.6 mm, 5 μm) at 40 ℃ with an injection volume of 5 μL. The mobile phase composition was formic acid/methanol (40∶60, *V*/*V*) at a flow rate of 0.6 mL·min$^{-1}$.

## 2 Results and discussion

### 2.1 Characterization

#### 2.1.1 Morphology and structure of $MoSe_2/Ag_3PO_4$ composites

Fig. 1 shows the morphology and structure of the $Ag_3PO_4$, $MoSe_2$, $MoSe_2/Ag_3PO_4$ and the used $MoSe_2/Ag_3PO_4$, respectively. Fig. 1a shows the well-dispersed $Ag_3PO_4$ particles with average size of 50 nm. Fig. 1b displays the $MoSe_2$ micro-flower balls. It is clearly showing that the micro-flower ball was composed of sheet structure. Fig. 1c reveals the SEM image of $MoSe_2/Ag_3PO_4$ binary composites containing the $Ag_3PO_4$ nanoparticles and $MoSe_2$ micro-flowers. After the introduction of $MoSe_2$ in the system, the $Ag_3PO_4$ particles size was 40 nm, which would be attributed to hydroxyl and carboxyl groups on $MoSe_2$ basal planes and edges that could easily confine the nucleation of $Ag_3PO_4$ nanoparticles and the growth of $Ag_3PO_4$ nanoparticles on its surface. The size of composite was reduced, thereby the specific surface area was increased and the contact area with the catalyst was expanded, which increased the photocatalytic efficiency. Fig. 1d indicates that the composite material had no obvious change after use.

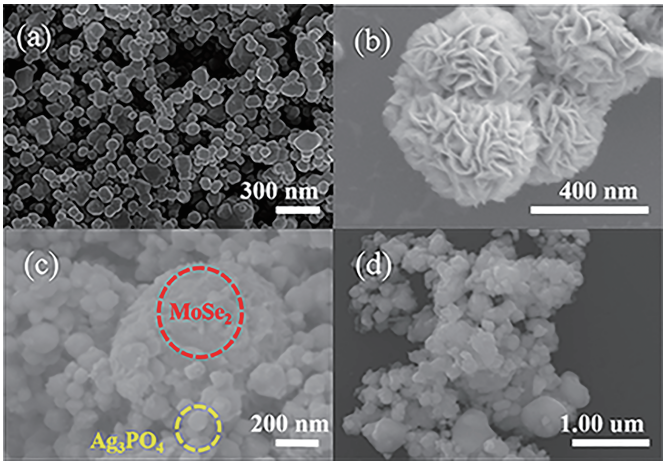


Fig.1 SEM images of $Ag_3PO_4$ (a), $MoSe_2$ (b), $MoSe_2/Ag_3PO_4$ (c) and the used $MoSe_2/Ag_3PO_4$ (d)

#### 2.1.2 XRD analysis

Fig. 2 shows the XRD patterns of $MoSe_2$, $Ag_3PO_4$, $MoSe_2/Ag_3PO$ and the used $MoSe_2/Ag_3PO_4$, respectively. As shown in curve (a), characteristic peak at 13.7°, 31.9°, 38.0° and 56.2° correspond to (002), (100), (103) and (110) crystal planes of $MoSe_2$[29]. As shown in curve (c), the characteristic peak at 21.9°, 29.7°, 33.3°, 36.6°, 42.5°, 47.8°, 52.7°, 55.2°, 57.3°, 62.1°, 69.9°, 71.9° and 73.9° correspond to (110), (200), (210), (211), (220), (310), (222), (320), (321), (400), (420), (421) and (332) crystal planes of $Ag_3PO_4$, respectively[30-33]. All peaks of $Ag_3PO_4$ correspond to the cubic crystal structure according to the standard card (PDF No. 06-0505). There was no impurity peak indicating that the $Ag_3PO_4$ prepared by this method was very pure. As shown in Fig. 2, the characteristic peak of $MoSe_2$ was not obvious, while that of $Ag_3PO_4$ was obvious.

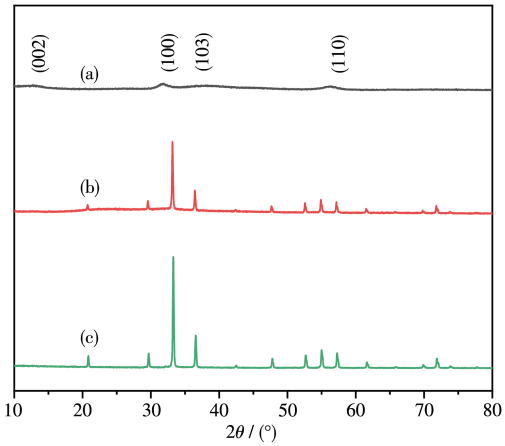


Fig.2 XRD patterns of $MoSe_2$ (a), $MoSe_2/Ag_3PO_4$(b), and $Ag_3PO_4$ (c)

Therefore, the peak of $Ag_3PO_4$ was dominant in the composites, and the weaker $MoSe_2$ was covered by $Ag_3PO_4$. So, no obvious characteristic peak of $MoSe_2$ can be seen in the XRD patterns of binary complexes. The XRD patterns can confirm that the introduction of $MoSe_2$ made little difference on $Ag_3PO_4$ crystalline structure. The well-dispersed $Ag_3PO_4$ particle, both in the pristine and nanocomposite samples, exhibited a high degree crystallinity.

2.1.3　XPS analysis

Fig.3a shows the XPS survey spectrum of $MoSe_2/Ag_3PO_4$, and peaks of Ag, P, Mo, Se and O element appeared in the binary $MoSe_2/Ag_3PO_4$ composites. The binding energy of O1*s* in Fig.3b was 531.7 eV, corresponding to the valence of −2, which indicated that O was derived from $Ag_3PO_4$. In Fig.3c, the binding energy of P2*p* was 132.9 eV, and the corresponding element valence is +5. As exhibited in Fig.3d, the characteristic peak at 54.2 and 55.3 eV could be seen, corresponding to Se3$d_{3/2}$. The corresponding element valence is −2. In Fig.3e, Mo3$d_{5/2}$ and Mo3$d_{3/2}$ are corresponded to 228.7 and 231.5 eV, respectively, which indicated that Mo is +4. The appearance of valences indicated the presence of $MoSe_2$ in the complex. In Fig.3f, the binding energies of Ag3$d_{2/3}$ and Ag3$d_{5/2}$ were located at 373.5 and 367.5 eV, respectively, indicating that the valence of the Ag ion is +1[34-35]. The above results proved the formation of $MoSe_2/Ag_3PO_4$.

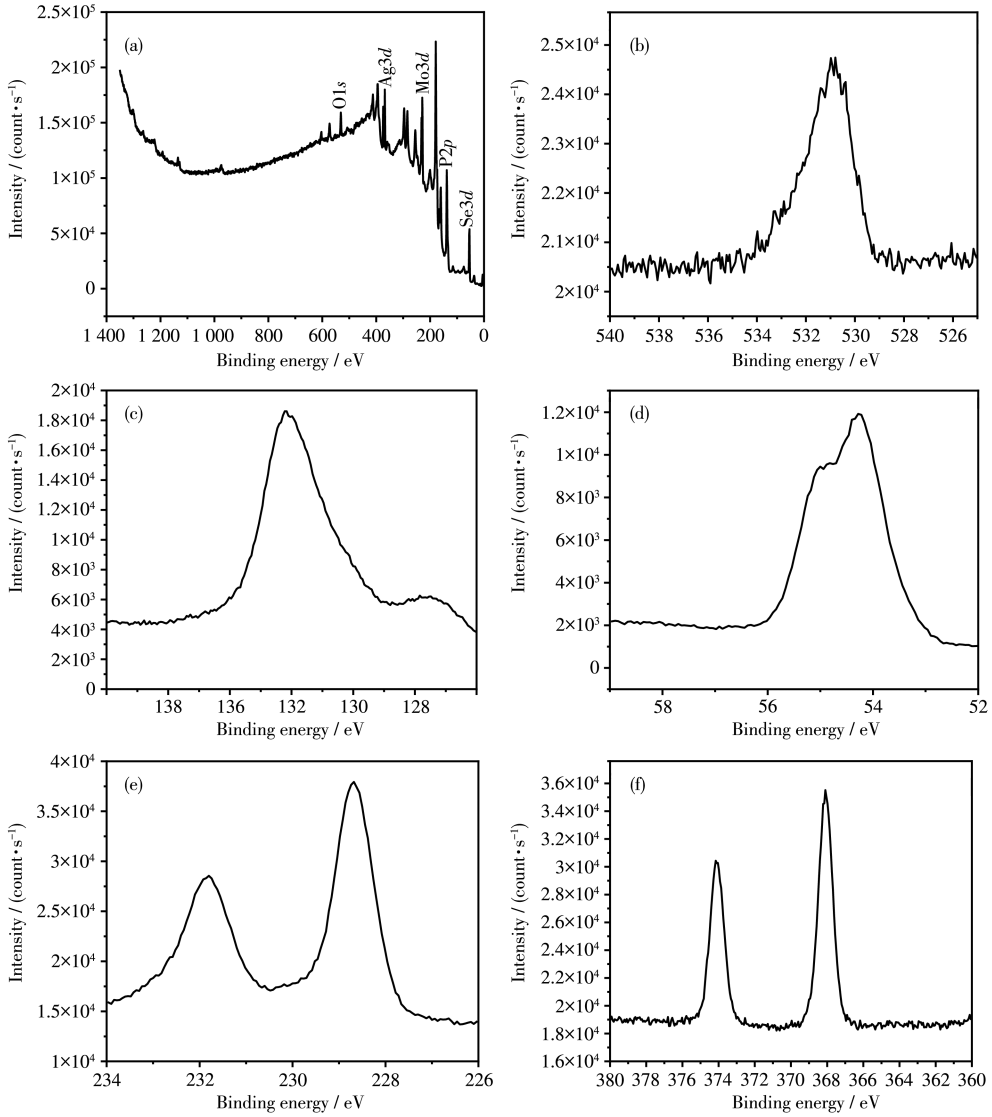


Fig.3　XPS spectra of $MoSe_2/Ag_3PO_4$: survey (a), O1*s* (b), P2*p* (c), Se3*d* (d), Mo3*d* (e) and Ag3*d* (f)

2.1.4 UV-Vis absorption spectra of $MoSe_2/Ag_3PO_4$ composites

Fig. 4a shows the UV - Vis spectra of $MoSe_2$, $Ag_3PO_4$ and $MoSe_2/Ag_3PO_4$, to study their optical absorption properties, respectively. The light absorbing boundary of single $Ag_3PO_4$ was located at 543 nm. When the $MoSe_2$ was introduced in the system to form the binary $MoSe_2/Ag_3PO_4$, the light absorption range was obviously enhanced that accounted for excellent visible light absorption of $MoSe_2$, which significantly improved the visible light adsorption for effective target pollute degradation. To gain some insights into the migration and separation of photogenerated carriers in the photocatalyst, photo - electrochemical characterizations (photocurrent responses and electrochemical impedance spectra, EIS) were carried out[36]. As shown in Fig.4b, the $MoSe_2/Ag_3PO_4$ performed the highest photocurrent intensity. For semicircle diameter in EIS Nyquist plot, the smaller semicircle diameter shows the lower resistance. In Fig.4c, we can see that the $MoSe_2/Ag_3PO_4$ had more efficient photogenerated electron transfer.

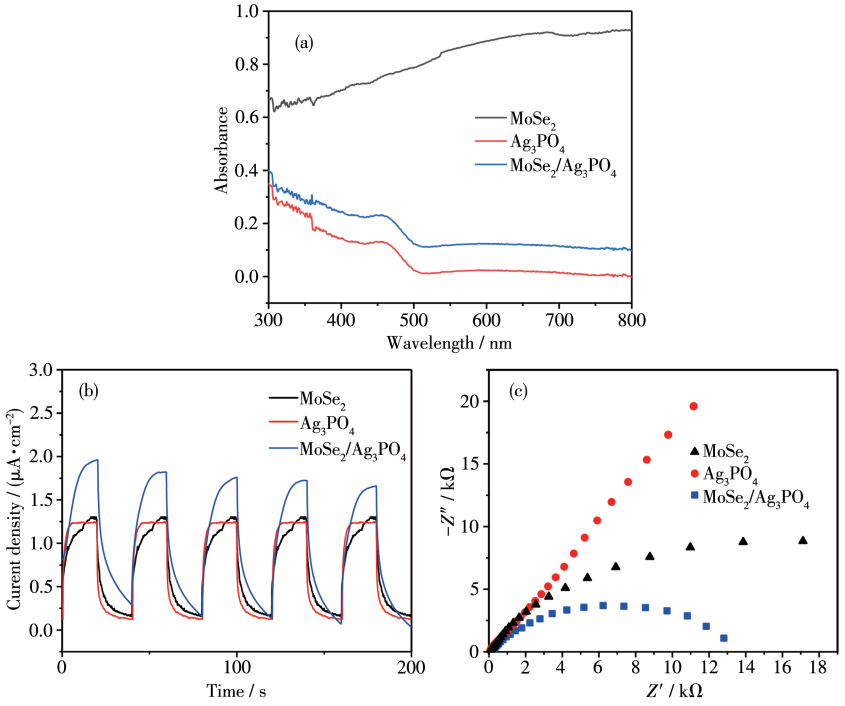


Fig.4 UV-Vis diffuse absorption spectra (a), photocurrent response density (b) and EIS spectra of $MoSe_2$, $Ag_3PO_4$ and $MoSe_2/Ag_3PO_4$ under visible light (c)

## 2.2 Photocatalytic experiment

2.2.1 Effect of ratios on photocatalysis

Fig.5a shows the catalytic activity of binary $MoSe_2/Ag_3PO_4$ with different mass ratios for RhB (10 $mg\cdot L^{-1}$) degradation under visible light irradiation. We found that the introduction of $MoSe_2$ could enhance the RhB degradation efficiency, and the champion combination of the $MoSe_2$ and $Ag_3PO_4$ (1∶5) could reach to 98% for RhB degradation under visible light irradiation within 30 min. The photocatalytic efficiencies of the composites were greater than those of the pure $Ag_3PO_4$, demonstrating that the photocatalytic performance of the composites is better than that of the monomer $Ag_3PO_4$[37]. When the dark reaction occurred for the first 30 min, pure $Ag_3PO_4$ had almost no effect on the removal of RhB, and all proportions of $MoSe_2/Ag_3PO_4$ materials had obvious adsorption effect on RhB. The reason was that the prepared $Ag_3PO_4$ had a smooth surface and poor adsorption performance, when the content of $MoSe_2$ increased, the flower - like structure of $MoSe_2$ showed good adsorption performance, and the adsorption of dye molecules on the surface was very good. After the adsorption tended to balance, the photocatalysis played a major role. However, when the $MoSe_2$ ratio

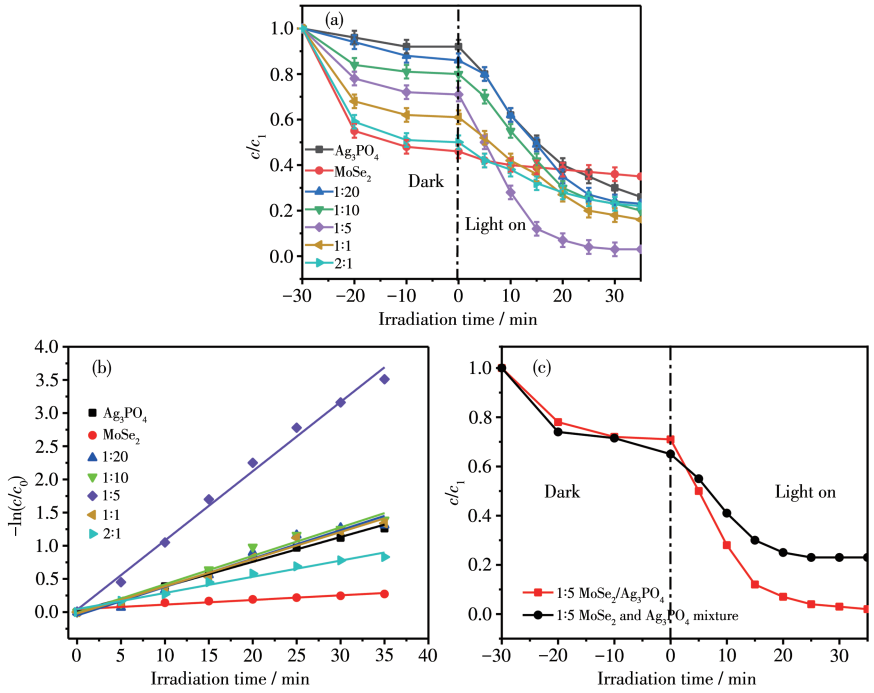


Quality of catalyst: 10 mg; initial concentration of RhB: 10 mg·$L^{-1}$; volume of solution: 100 mL; pH: neutral; temperature: room temperature

Fig.5　Photocatalytic reduction of RhB by $Ag_3PO_4$ and different mass ratios of $MoSe_2/Ag_3PO_4$ (a), fitted linear equations (b) and comparison of degradation of $MoSe_2/Ag_3PO_4$ (1∶5) and mechanical mixture of $MoSe_2$ and $Ag_3PO_4$ (1∶5) (c)

was too large, $MoSe_2$ could wrap on the surface of $Ag_3PO_4$, resulting in a decrease in light transmission performance, which affected degradation efficiency. When the mass ratio of $MoSe_2$ to $Ag_3PO_4$ was 1:5, the complex degraded the target pollutant at the highest rate. Fig. 5b shows the kinetic constants ($k$) of the as prepared products. The $k$ value of $MoSe_2/Ag_3PO_4$ composite (1∶5) (0.122 5 $min^{-1}$) was 3.1 times higher than that of pristine $Ag_3PO_4$ (0.039 5 $min^{-1}$). As shown in Fig. 5c, the photocatalytic reduction of RhB by $MoSe_2/Ag_3PO_4$ composite was better than that by mechanical mixing. In the dark reaction stage, due to the complex of $MoSe_2$ and $Ag_3PO_4$, the adsorption sites of $MoSe_2$ became less and the adsorption effect became worse.

### 2.2.2　Effect of pH on photocatalysis

The pH in the printing and dyeing wastewater is not a fixed value in actual use. By changing the pH of the RhB, the degradation effect in the actual use process was simulate. The pH of the dye solution was adjusted to 5, 6, 7, 8, and 9 using hydrochloric acid and sodium hydroxide. In Fig.6a, the final photocatalytic efficiency was 98% at any pH. However, with the

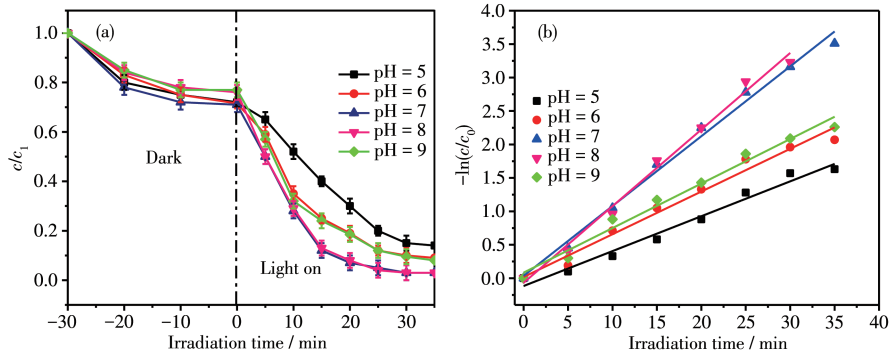


Quality of catalyst:10 mg; initial concentration of RhB: 10 mg·$L^{-1}$; volume of solution: 100 mL; temperature: room temperature

Fig.6　Degradation effect of different pH values (a) and fitted linear equations (b)

decrease of pH, it took longer to reach the photocatalytic endpoint (pH<7). The degradation rate was faster, and the degradation end could reach about 30 min of light when pH>7. The reason is that the solution is acidic and contains a large amount of $H^+$ when pH<7, which makes $MoSe_2$ surface presence a large number of cations. RhB is a cationic type of dye, which also has a positive charge in the solution. The molecules and the adsorbent will repel each other, and the presence of $H^+$ will compete with the dye for adsorption, so the enrichment of the dye molecules on the catalyst surface will be reduced, so it takes longer to reach the end of degradation. The $H^+$ concentration in the liquid gradually decreases when pH>7, the electrostatic effect gradually weakens, and the competitive adsorption slowly weakens, so the photocatalytic degradation end will come earlier than before. Fig.6b shows the fitted linear equations for the different pH values of RhB, and the variations of $k$ value was similar to photocatalytic efficiency.

2.2.3 Effect of RhB concentration on photocatalysis

The initial concentration of pollutants has a great impact on the degradation efficiency. We have configured dyes with a concentration of 5, 10, 15, 20 and 25 mg·L$^{-1}$, respectively. $MoSe_2/Ag_3PO_4$ composite (1∶5) was used for degradation experiments. As shown in Fig.7a, when the dye concentration was low (5 mg·L$^{-1}$), the dark reaction part removed most of the dye molecules. After 30 min of visible light irradiation that the final degradation rate was above 99%. As the dye concentration increased, the degradation rate dropped dramatically. When the RhB dye concentration was as high as 25 mg·L$^{-1}$, only 34% of the dye degraded after 30 min of light exposure. Since the dye concentration was too large, the chromaticity of the solution increased, resulting in a decrease in the transmittance of the solution, hindering the transmittance of light, resulting in a decrease in photocatalytic efficiency. The linear fitting equation and kinetic constants ($k$) of $MoSe_2/Ag_3PO_4$ obtained with different RhB concentrations are shown in Fig.7b, and the $k$ value of 10 mg·L$^{-1}$ (0.122 5 min$^{-1}$) was 11.67 times higher than that of 25 mg·L$^{-1}$ (0.010 5 min$^{-1}$).

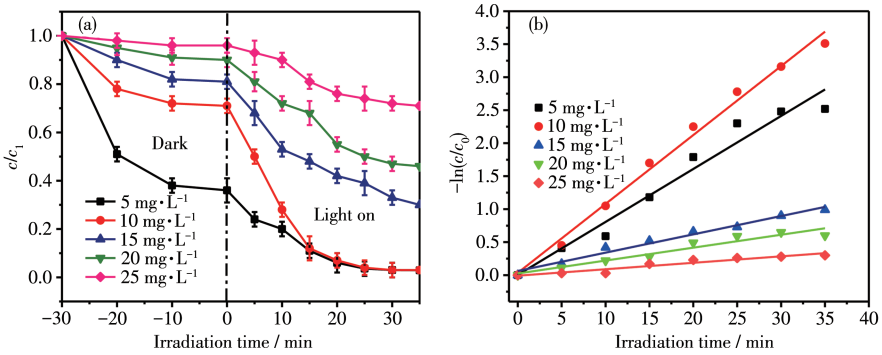


Quality of catalyst:10 mg; volume of solution: 100 mL; pH: neutral; temperature: room temperature

Fig.7 Effect of different concentrations on degradation (a) and fitted linear curves (b)

2.2.4 Effect of temperature on photocatalysis

The temperature of printing and dyeing wastewater is generally very high, but temperature has a great influence on photocatalytic system. If the temperature of the water is too low, it will cause the company′s cooling equipment to occupy too much space and increase the treatment cost. By changing the water temperature (15, 20, 25, 30, 35 and 40 ℃) of RhB dye, the degradation effect in actual use was simulated. $MoSe_2/Ag_3PO_4$ composite (1∶5) was used for degradation experiments. In Fig. 8a, the degradation rate of RhB (10 mg·L$^{-1}$) could reach 98% at different temperatures, which was consistent with the previous experimental results, but the time to reach the end of degradation was different. When the reaction temperature was 15 ℃, it took 35 min to complete the reaction, but when the temperature was increased, the degradation end came early, only 25 min at 20 ℃. When the temperature continued to rise, the reaction rate continued to decline. When the water temperature reached 40 ℃, it took more than 45 min to degrade 98.2% of the dye. Although it is conducive to the photocatalytic reaction, too low temperature could

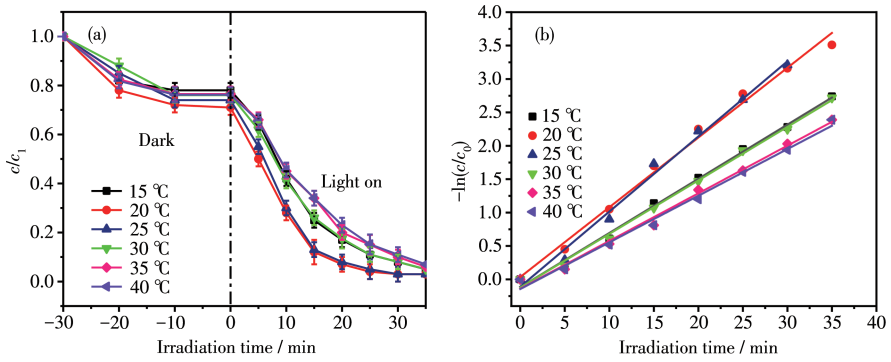


Quality of catalyst:10 mg; initial concentration of RhB: 10 mg·$L^{-1}$; volume of solution: 100 mL; pH: neutral

Fig.8　Effect of different temperatures on degradation (a) and fitted linear curves (b)

also cause the thermal motion of the molecules to slow down when the water temperature was lower than room temperature. The stirring speed must also be increased accordingly to ensure that the dye molecules and the photocatalyst were in full contact. When the temperature was too high, the speed of molecular thermal motion was accelerated, but the dissolved oxygen content in water could be reduced, and the amount of $\cdot O_2^-$ generated by light excitation could be reduced accordingly, affecting the photocatalytic efficiency. Most of the dye wastewater is high temperature, and the discovery of this experimental phenomenon has practical application value. Based on this phenomenon, we can appropriately increase the temperature of the photocatalytic reaction and reduce the area and cost of the cooling equipment. Fig.8b shows the fitted linear curves at different temperatures of RhB, and the $k$ value at 20 ℃ (0.145 3 $min^{-1}$) was 2.02 times higher than that of 40 ℃ (0.072 $min^{-1}$).

### 2.2.5　Cyclic test

It is worth to point out that the stability of the photocatalysts plays a significant role in its practical application. Since $Ag_3PO_4$ is unstable and can be easily corroded by visible-light irradiation because of the reduction of silver ions ($Ag^+$) to silver (Ag) by the photogenerated electrons if no sacrificial reagent is involved. As shown in Fig.9a, the pure $Ag_3PO_4$ catalyst showed poor stability for RhB degradation after 4 cycles run (cumulative use of 280 min), only remaining 5% of the degradation rate. At the same time, the binary composite obtained with the mass ratio of 1∶5 came with no apparent decline, and the degradation rate remained 89%. It is implied that the composite photocatalysis had good cycle stability. From Fig.9b, it can be seen that there was no obvious change in the XRD pattern of the $MoSe_2/Ag_3PO_4$ composite before and after use except at 37°. The impurity peak of the composite at about 37° was the peak of Ag produced by $Ag_3PO_4$ in the case of

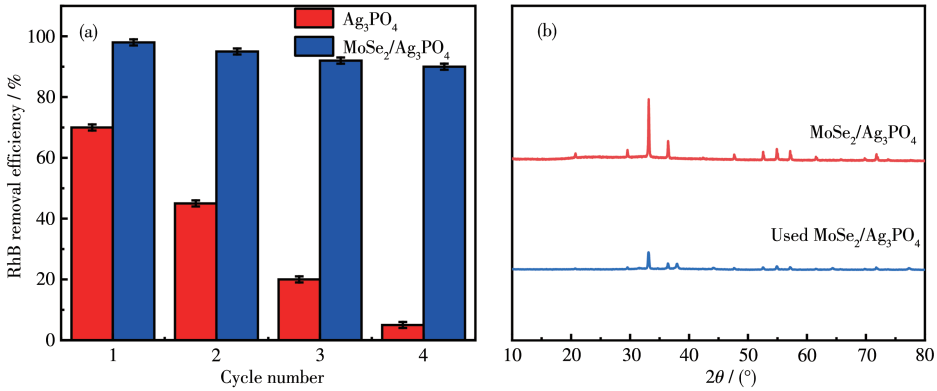


Fig.9　Photo-stability of $Ag_3PO_4$ and $MoSe_2/Ag_3PO_4$ by investigating its photocatalytic activity with three times of cycling use (a) and XRD comparison of $MoSe_2/Ag_3PO_4$ before and after use (b)

illumination.

2.2.6 Analysis of the degradation intermediates

To explore the photodegradation products of RhB, the reaction intermediates during the photocatalytic process were detected by LC/MS technique. The absorption spectrum changed with time evolution during the photocatalytic degradation of RhB in $MoSe_2/Ag_3PO_4$ composites obtained with the mass ratio of 1:5 is illustrated in Fig. 10. It was found that in the presence of the $MoSe_2/Ag_3PO_4$ photocatalyst, the color of the suspension became colorless after 35 min. To further explore the degradation process of RhB, the main intermediate products of RhB degradation were identified by LC/MS technology, and the molecular-ion and fragment-ions of N-de-ethylated intermediates are shown in Table S1 and Fig. S1. Combining the measured intermediate products, a possible degradation pathway of RhB is demonstrated in Fig. 11. The photocatalytic degradation of RhB dyes mainly included two competitive pathways: N-de-ethylation and the cleavage of the conjugated structure[38-40]. Firstly, RhB (*m*/*z*=443) was readily attacked by $h^+$ and $\cdot O_2^-$ free radicals, so that the ethyl group was broken and converted into *N*-(9-(2-carboxyphenyl)-6-(ethylamino)-3*H*-xanthen-3-ylidene)-*N*-ethylethanaminium (*m*/*z*=415) and *N*-(6-amino-9-(2-carboxyphenyl)-3*H*-xanthen-3-ylidene) *N*-ethylethanaminium (*m*/*z*=387). As the decomposed carbon-nitrogen bond splits further, it formed 9-(2-carboxyphenyl)-6-(ethylamino)-3*H*-xanthen-3-iminium (*m*/*z*=359) and 6-amino-9-(2-carboxyphenyl)-3*H*-xanthen-3-iminium (*m*/*z*=331). Subsequently, 6-amino-9-(2-carboxyphenyl)-3*H*-xanthen-3-iminium (*m*/*z*=331) was decomposed into smaller molecules (6-amino-9-phenyl-cyclopenta-chromenylium, *m*/*z*=258) by that the carboxyl group immediately fell off and the conjugated structure quickly collapsed. Eventually, the intermediate product was broken down into smaller molecules ((cyclohexa-2,5-dien-1-ylidenemethylene) dibenzene,

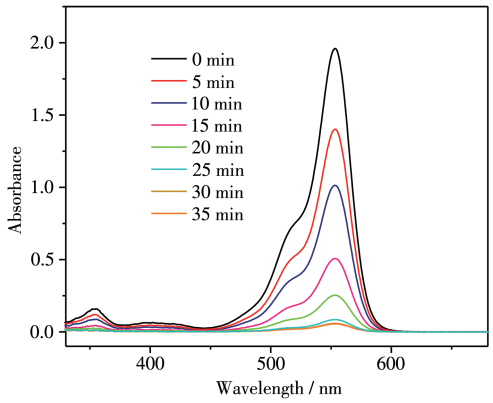


Fig.10 UV-Vis absorption spectrum of the RhB degradation over the as-synthesized $MoSe_2/Ag_3PO_4$ nanospheres under visible light irradiation

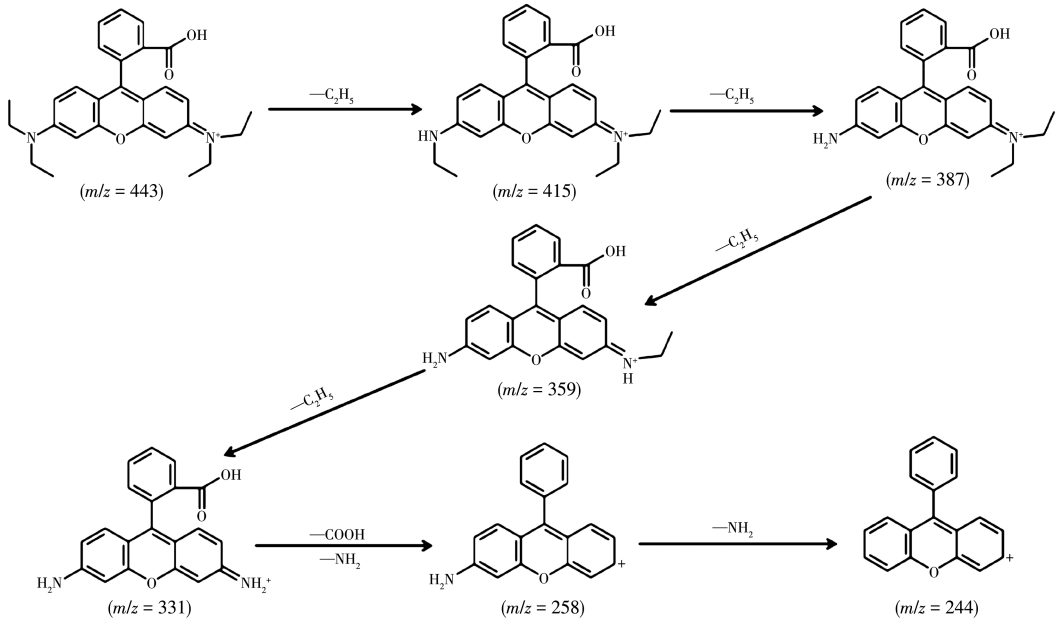


Fig.11 Possible pathways followed during the RhB photodegradation

*m*/*z*=244). As chromophores such as azo bond presented in RhB gradually cleaved completely, the solution changed from rose red to colorless.

2.2.7　Photocatalytic mechanism

The active species in the degradation of RhB could be determined by trapping experiments in $MoSe_2/Ag_3PO_4$. Ammonium oxalate, benzoquinone and 2-propanol were employed to capture holes ($h^+$), superoxide radical ($\cdot O_2^-$) and hydroxyl radical ($\cdot OH$), respectively. As shown in Fig.12, after adding ammonium oxalate, the final degradation rate decreased to 39.7%. When benzoquinone was present, the degradation rate was still 61.5%. When 2-propanol was added to the system, the degradation rate was as high as 89.4%. Thus, we can draw a conclusion that $h^+$ plays the main role in RhB degradation, immediately followed by $\cdot O_2^-$ and $\cdot OH$ active species. We utilize electronspin-resonance spectroscopy (ESR) to verify the $\cdot O_2^-$ generated in the photocatalytic process. In Fig.12b, no ESR signals could be found under dark condition. However, under visible light irradiation, the characteristic signal of $\cdot O_2^-$ appeared, and with the increase of irradiation time (from 3 to 8 min), the signal intensity gradually increased, which revealed that $\cdot O_2^-$ could be generated in the photocatalytic degradation reaction and participate in the photocatalytic degradation reaction[41-43].

Based on the results of the reactive-species-trapping experiments and ESR spectra, the possible degradation mechanisms of the $MoSe_2/Ag_3PO_4$ composite was studied and shown in Fig.13. Owing to different potentials of $MoSe_2$ ($E_{CB}$=−0.93 eV and $E_{VB}$=0.98 eV) and $Ag_3PO_4$ ($E_{CB}$=0.29 eV and $E_{VB}$=2.64 eV), where $E_{CB}$ and $E_{VB}$ are the conduction and valance band edge potentials, it is obvious that the CB and VB of $MoSe_2$ were higher than that of $Ag_3PO_4$, respectively. Normally, two photo-degradation mechanisms may be proposed (conventional type Ⅱ mechanism and Z-scheme mechanism). However, the charge transfer pathway of this work does not conform to the type Ⅱ mechanism. This is because the electrons on the CB of $Ag_3PO_4$ cannot

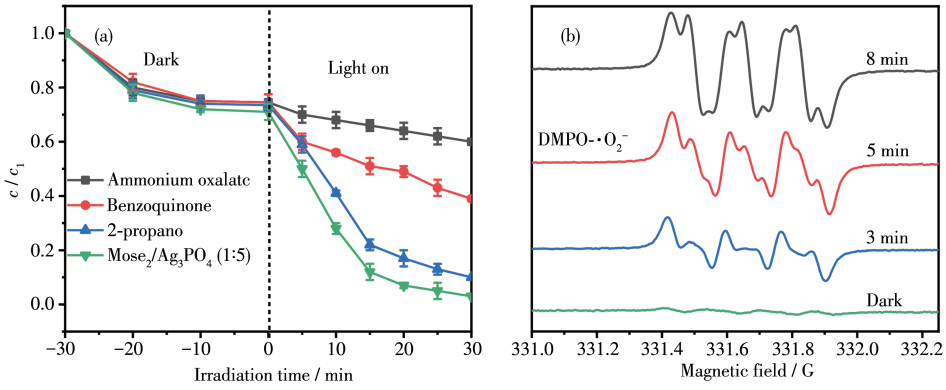


Fig.12　Reactive-species-trapping experiments (a) and ESR spectra of $MoSe_2/Ag_3PO_4$ for detecting $\cdot O_2^-$ under the visible light irradiation (b)

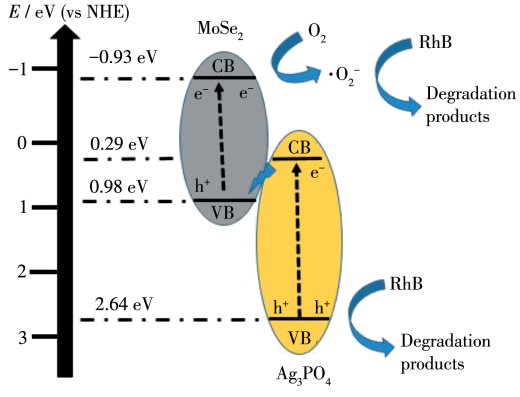


Fig.13　Possible photocatalytic degradation mechanisms of RhB by $MoSe_2/Ag_3PO_4$

reduce $O_2$ to yield $\cdot O_2^-$ (more positive potential of the CB of $Ag_3PO_4$ than $O_2/\cdot O_2^-$, −0.33 eV). Conversely, $\cdot O_2^-$ is the main active species, implying the electrons on the CB of $MoSe_2$ react with $O_2$ to produce $\cdot O_2^-$. Therefore, Z-scheme mechanism is more reasonable for the prepared composite. As shown in Fig.13, under the excitation of visible light, the electrons present in the VBs of $MoSe_2$ and $Ag_3PO_4$ are excited to their CBs, respectively, leaving $h^+$ on their VBs. For one thing, the electrons in the CB of $Ag_3PO_4$ combine with the holes on the VB of $MoSe_2$. For another, the electrons in the CB of $MoSe_2$ readily move to its surface to reduce $O_2$ to $\cdot O_2^-$, and holes leaving in the VB of $Ag_3PO_4$ will directly oxidize RhB to form corresponding degradation products.

## 3 Conclusions

Successfully synthesized binary $MoSe_2/Ag_3PO_4$ composite photocatalyst was employed for RhB degradation under visible light irradiation. $Ag_3PO_4$ acted as the photosensitizer for visible light adsorption and $MoSe_2$ was introduced to protect $Ag_3PO_4$ from photocorrosion and simultaneously acted as electron acceptor favorable for effective $e^- - h^+$ separation. The catalytic capability of binary $MoSe_2/Ag_3PO_4$ composite was evaluated by degradation of RhB and the degradation rate could reach to 98% after 30 min under visible light irradiation. $MoSe_2/Ag_3PO_4$ achieved 89% of the degradation under visible light irradiation after four regenerations. The active species in the degradation process were studied by trapping experiments, and it was found that both $h^+$ and $\cdot O_2^-$ play important roles in the degradation process. Overall, this work not only provides an effective and simple approach to fabricate an $Ag_3PO_4$-based binary heterojunction system, but also gives deeper insight into the mechanism for efficient visible-light photodegradation, which enables us to establish a strategy to design better photocatalysts.

Supporting information is available at http://www.wjhxxb.cn

Acknowledgments: This study was funded by the Natural Science Foundation of China (Grant No. 51908252), the China Postdoctoral Science Foundation (Grant No. 2019M652274), the Postdoctoral Preferred Funding Project of Jiangxi (Grant No. 2019KY17), the Postgraduate Research & Practice Innovation Program of Jiangsu Province (Grant No. SJCX19_1198), the Social Development Project of Zhenjiang (Grant No. 2016014), the Qing Lan Project for Young Core Teachers in University of Jiangsu Province, and the Foundation from Marine Equipment and Technology Institute for Jiangsu University of Science and Technology (Grant No. HZ20190004).

## References:

[1] Fujishima A, Honda K. *Nature*, **1972**,**238**:37-38

[2] Harir M, Gaspar A, Kanawati B, Fekete A, Frommberger M, Martens D, Kettrup A, El Azzouzi M, Schmitt-Kopplin P. *Appl. Catal. B*, **2008**, **84**:524-532

[3] 杨传锋, 腾伟, 宋艳华, 崔言娟. 催化学报, **2018**,**39**:1615-1624
YANG C F, TENG W, SONG Y H, CUI Y J. *Chin. J. Chem.*, **2018**,**39**: 1615-1624

[4] Montoya J F, Velásquez J A, Salvador P. *Appl. Catal. B*, **2009**,**88**:50-58

[5] Lin Y X, Ferronato C, Deng N S, Chovelon J M. *Appl. Catal. B*, **2011**, **104**:353-360

[6] Wang H J, Chen X Y. *J. Hazard. Mater.*, **2011**,**186**:1888-1892

[7] Vaiano V, Iervolino G. *J. Colloid Interface Sci.*, **2018**,**518**:192-199

[8] Baia L, Orbán E, Fodor S, Hampel B, Kedves E Z, Saszet K, Szekely I, Karacsonyi E, Reti B, Berki P, Vulpoi A, Magyari K, Csavdari A, Bolla C, Cosoveanu V, Hernadi K, Baia M, Dombi A, Danciu V, Kovacs G, Pap Z. *Mater. Sci. Semicond. Process*, **2015**,**42**:66-71

[9] Kalikeri S, Kamath N, Gadgil D J. *Environ. Sci. Pollut. Res.*, **2017**,**25**: 3731-3744

[10] Yi Z G, Ye J H, Kikugawa N, Kako T, Ouyang S, Stuart-Williams H, Yang H, Cao J Y, Luo W J, Li Z S. *Nat. Mater.*, **2010**,**9**:559-564

[11] Wang H, Bai Y S, Yang J T, Lang X F, Li J H, Lin G. *Chem. Eur. J.*, **2012**,**18**:5524-5529

[12] Ge M, Zhu N, Zhao Y P, Li J, Liu L. *Ind. Eng. Chem. Res.*, **2012**,**51**: 5167-5173

[13] Wang K, Hua X, Xu J. *J. Mol. Catal. A*: *Chem.*, **2014**,**393**:302-308

[14] Bian L L, Liu Y J, Zhu G X, Yan C, Zhang J H, Yuan A H. *Ceram. Int.*, **2018**,**44**:7580-7587

[15] Yang J H, Yao H X, Liu Y Q, Zhang Y J. *Nanoscale Res. Lett.*, **2008**, **3**:481-485

[16] Voiry D, Yamaguchi H, Li J W, Silva R, Alves D C B, Fujita T S, Chen M W, Asefa T, Shenoy V B, Eda G. *Nat. Mater.*, **2013**,**12**:850-855

[17] Li X, He X Y, Shi C M, Liu B, Zhang Y Y, Wu S Q, Zhu Z Z, Zhao J B. *ChemSusChem*, **2014**,**7**:3328-3333

[18] Teng W, Tan X J, Li X Y, Tang Y B. *Appl. Surf. Sci.*, **2017**,**409**:250-260

[19] Li Y, Xiao X Y, Ye Z H. *Appl. Surf. Sci.*, **2019**,**468**:902-911

[20] Liu R D, Li H, Duan L B, Shen H, Zhang Q, Zhao X R. *Appl. Surf. Sci.*, **2018**,**462**:263-269

[21]Wang W W, Wang L, Li W B, Feng C, Qiu R, Xu L K, Cheng X D, Shao G Q. *Mater. Lett.*, **2019**,**234**:183-186

[22]Song H J, You S S, Jia X H. *Appl. Phys. A*: *Mater. Sci. Process.*, **2015**, **121**:541-548

[23]Shi W L, Guo F, Li M Y, Shi Y, Shi M J, Yan C. *Appl. Surf. Sci.*, **2019**,**473**:928-933

[24]Qi S Y, Liu X H, Zhao B C. 2014 *International Conference on Computer Science and Electronic Technology*. Guilin: Atlantis Press, China, **2015**:136-139

[25]Shaw J C, Zhou H L, Chen Y, Weiss N O, Liu Y, Huang Y, Duan X F. *Nano. Res.*, **2014**,**7**:511-517

[26]Bougouma M, Batan A, Guel B, Segato T, Legma J B, Reniers F, Ogletree M P D, Herman C B Doneux T. *J. Cryst. Growth*, **2013**,**363**: 122-127

[27]Helmly B C, Lynch W E, Nivens D A. *Spectrosc. Lett.*, **2007**,**40**:483-492

[28]Zhang X H, Xue H X, Wang J T. *Nano-Micro Lett.*, **2015**,**10**:339-342

[29]Kou S F, Guo X, Xu X F, Yang J. *Catal. Commun.*, **2018**,**106**:60-63

[30]Liu R D, Li H, Duan L B, Shen H, Zhang Q, Zhao X R. *Appl. Surf. Sci.*, **2018**,**462**:263-269

[31]Yan J, Song Z L, Wang X, Xu Y G, Pu W J, Xu H, Yuan S Q, Li H M. *Appl. Surf. Sci.*, **2019**,**466**:70-77

[32]Shi Y, Tang Y B, Chen F Y, Shi W L, Guo F, Wang X G. *Desalin. Water Treat.*, **2019**,**170**:287-296

[33]Song Y H, Zhao H Z, Chen Z G, Wang W R, Huang L Y, Xu H, Li H M. *Phys. Status Solidi A*, **2016**,**213**:2356-2363

[34]Kim Y G, Jo W K. *J. Hazard. Mater.*, **2019**,**361**:64-72

[35]Tang Y B, Yang H J, Chen F Y, Wang X G. *Desalin. Water Treat.*, **2018**,**110**:144-153

[36]Guo F, Li M Y, Ren H Q, Huang X L, Wang C, Shi W L, Lu C Y. *Appl. Surf. Sci.*, **2019**,**491**:88-94

[37]Dinh C T, Nguyen T D, Kleitz F, Do T O. *Chem. Commun.*, **2011**,**47**: 7797-7799

[38]Rasheed T, Bilal M, Iqbal H M N, Shah S Z H, Hu H B, Zhang X H, Zhou Y F. *Environ. Technol.*, **2018**,**39**:1533-1543

[39]Zhang L, He Y M, Wu Y, Wu T H. *Mater. Sci. Eng. B*, **2011**,**176**: 1497-1504

[40]Martínez-de la Cru A, GarcíaPérez U M. *Mater. Res. Bull.*, **2010**,**45**: 135-141

[41]Shi W L, Li M Y, Huang Q L, Ren H J, Guo F, Tang Y B, Lu C Y. *Chem. Eng. J.*, **2020**,**394**:125009

[42]Guo F, Huang Q L, Chen Z H, Sun H R, Shi W L. *Sep. Purif. Technol.*, **2020**,**253**:117518

[43]Guo F, Sun H R, Cheng L, Shi W L. *New J. Chem.*, **2020**,**44**:11215-11223